

CONFERENCES AND SYMPOSIA

PACS number: 01.10.Fv

Joint scientific session of the Physical Sciences Division of the Russian Academy of Sciences and the Joint Physical Society of the Russian Federation "Strongly correlated electrons in two-dimensional systems" (26 October 2005)

A joint scientific session of the Physical Science Division of the Russian Academy of Sciences and the Joint Physical Society of the Russian Federation was held on 26 October 2006 at the conference room of the Lebedev Physics Institute, RAS. The following reports were presented at the session.

(1) **Pudalov V M** (Lebedev Physics Institute, RAS) "Metal – insulator transitions and related phenomena in a strongly correlated two-dimensional electron system";

(2) **Iordanskii S V, Kashuba A** (Landau Institute for Theoretical Physics, RAS) "Two-dimensional multicomponent electron gas as a model for silicon heterostructures";

(3) **Olshanetskii E B** (Institute of Semiconductor Physics (ISP), RAS SB, Novosibirsk), **Renard V** (GHML, MPI-FKF/CNRS, Grenoble, France), **Kvon Z D** (ISP, RAS SB, Novosibirsk), **Gornyi I V** (Institut für Nanotechnologie, Karlsruhe, Germany; Ioffe Physical Technical Institute, RAS, St. Petersburg), **Toropov A I** (ISP, RAS SB, Novosibirsk), **Portal J C** (GHML, MPI-FKF/CNRS, Grenoble, France) "Interaction effects in the transport and magnetotransport of two-dimensional electrons in AlGaAs/GaAs and Si/SiGe heterojunctions."

Summaries of the reports are given below.

PACS numbers: **71.27.+a**, **71.30.+h**, 72.15.Rn
DOI: 10.1070/PU2006v049n02ABEH005921

Metal – insulator transitions and related phenomena in a strongly correlated two-dimensional electron system

V M Pudalov

1. Introduction: competition of quantum interference and dimensionality

Understanding the properties of two-dimensional (2D) electron systems in the presence of both strong interparticle interactions and disorder is an outstanding problem in condensed matter physics that is still far from being solved. The late 1970s witnessed the completion of the theory of quantum (i.e., wave) interference corrections for noninteracting electrons, according to which the quantum interference correction $\delta\sigma_{\rm qi}$ to the semiclassical Drude – Boltzmann value $\sigma_{\rm D}$ acts to decrease the conductivity σ and can be regarded as 'backscattering' [1 – 3]:

$$\sigma = \sigma_{\rm D} + \delta\sigma_{\rm qi} = \sigma_{\rm D} - \frac{e^2}{\pi h} \ln\left(\frac{\tau_\varphi}{\tau}\right) \approx \sigma_{\rm D} + \frac{e^2}{\pi h} \ln T .$$

While small in three dimensions, the quantum interference correction is of fundamental importance in 2D systems, where the conductance G is independent of size. As temperature decreases, the quantum correction increases logarithmically until it becomes comparable to $\sigma_{\rm D}$ and leads to localization, which implies an exponential decrease in the conductivity.

These were the ideas that led to the creation of the scaling theory of conductivity in 1979 [4]. According to this theory, localization develops as the quantum length scale increases and is a result of competition between quantum interference, disorder, and dimensionality. In particular, a 2D system of noninteracting electrons cannot have metallic conduction and must become an insulator at $T = 0$. Figure 1a below shows an example of such conductivity behavior for a strongly disordered (low-mobility) sample. It can be seen that at low electron concentration, the conductivity decreases exponentially with decreasing temperature, suggesting a strong localization in the system. As the density increases, a transition occurs to the regime in which the conductivity varies approximately logarithmically with the temperature. Just as the scaling theory of conductivity predicts, at no concentrations or temperatures does the conductivity show evidence for metallic behavior ($d\sigma/dT < 0$).

The theory of quantum corrections led to a major revision of the classical understanding of conductivity and (as reviewed in Refs [1, 2]) was brilliantly confirmed in numerous experimental studies on 3D metallic samples and metallic films that were available in the 1970 – 1980s and in which the electron – electron interaction is weak. Indeed, the nearly 15-year dominance of the scaling theory misled researchers to believe that it is universal and works equally well when the interparticle interaction is strong.

Over the years, with advances in semiconductor technologies and the fabrication of increasingly pure samples with 2D electron layers, 2D electron systems with much lower concentrations have become available to study. In the low-concentration limit, electrons in an ideally pure system must form a Wigner crystal [5 – 7]. At higher densities, the electron system remains in the 'liquid' state and is characterized by strong electron – electron correlations. Such a strongly 2D system can exhibit new quantum states different from those

Uspekhi Fizicheskikh Nauk **176** (2) 213 – 227 (2006)
Translated by E G Strel'chenko; edited by A M Semikhatov

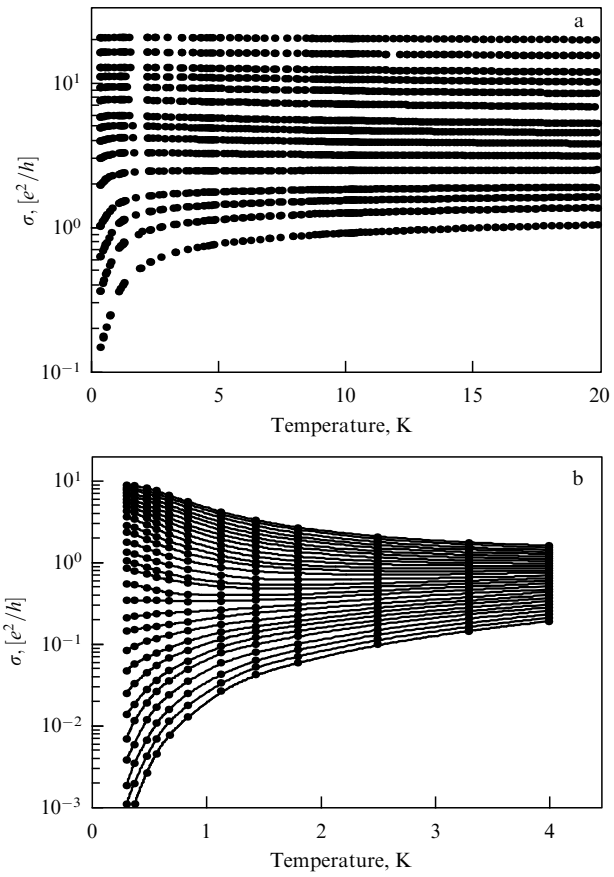

Figure 1. The temperature dependence of the conductivity of a 2D electron system in silicon in the absence of a magnetic field: (a) for a sample with a low mobility of 0.15 m^2 $(V\ s)^{-1}$, the curves, from bottom up, are for the following electron densities (in units of 10^{11} cm^{-2}): 3.85, 4.13, 4.83, 5.53, 6.23, 7.63, 9.03, 10.4, 11.8, 13.2, 16.0, 18.8, 21.6, 24.4, 30.0, 37.0; (b) for a sample with a high mobility of 3.62 m^2 $(V\ s)^{-1}$ [16], the curves are for electron densities that vary (from bottom up) from 0.717 to 1.326 in steps of 0.0218.

known for noninteracting electrons — which is very attractive to both theorists and experimenters.

The universal applicability of scaling theory was directly compromised in the early 1990s when studying the transition of an electron liquid from the state with quantized Hall resistance to the insulator state [8 – 11]. The experiments revealed, namely, that localized states that lie at the centers of the disorder-broadened Landau levels in the strong-magnetic-field quantum-Hall-effect regime merge and remain in a finite energy interval as the magnetic field H decreases. This contradicts the scaling theory prediction that delocalized states rise in energy and move across the Fermi level as $H \to 0$ [12, 13]. Furthermore, in a direct challenge to the one-particle scaling theory, the subsequent studies of conductivity in the absence of a magnetic field provided evidence for metallic transport and the metal-to-insulator transition in 2D systems of electrons in high-mobility Si structures.

Figure 1b shows typical temperature behavior of conductivity for pure (high-mobility) samples [16]. It is seen that at low densities, the curves $\sigma(T)$ differ little from the corresponding curves in Fig. 1a and demonstrate hopping conductivity, the usual behavior for a strongly localized state. But above a certain critical density n_c (in our case, $n_c = 0.96 \times 10^{11}$ cm^{-2}), $\sigma(T)$ shows a sharply different temperature dependence: similarly to what happens in an ideal metal, the conductivity starts to increase rapidly with decreasing temperature. Two branches of the dependence $\sigma(T)$ (the 'metallic' for $n > n_c$, and the 'insulating' for $n < n_c$) are mirror-symmetric with respect to $\sigma(n_c)$ [15] — akin to the symmetry the conductivity of 3D systems shows at the metal – insulator transition. A standard scaling analysis of these curves shows [15] that the experimental $\sigma(T)$ curves for $n > n_c$ and those for $n < n_c$ can indeed be reduced to two universal dependences $\sigma(T)_{i=1,2} \propto \exp(\pm T_0/T)$ in which the scaling parameter T_0 shows the critical behavior $T_0 \propto (n - n_c)^{-p}$ near n_c.

Experimental finding of new physics in the field where it was not expected provided a major stimulus for subsequent studies, both theoretical and experimental, of strongly correlated 2D systems. Metallic conductivity and the metal – insulator transition were similarly found in a variety of 2D systems, including 2D electron layers in GaAs/AlGaAs, InAs/GaAs, *n*-AlAs, Si/SiGe and inverted silicon metal – insulator – semiconductor (Si-MOS) structures, and 2D hole layers in GaAs/AlGaAs and Si/SiGe (see reviews [17 – 21] and the references therein). In all the cases studied, the metal – insulator transition occurs with decreasing the electron density, when the system's conductance reaches a value of the order of e^2/h [17 – 19]. Is the observed effect a true quantum transition and is the metallic state of a 2D system its ground state (at $T = 0$)? Or does the conventional physics of disordered and interacting electrons suffice to settle things? These fundamental questions are stimulating interest in this field.

2. Quantitative study of the e – e interaction

Because the critical behavior of conductivity as shown in Fig. 1b contradicts the expectations for noninteracting electrons, various types of interaction were analyzed theoretically for their possible effects. It was found that the spin – orbit interaction — even though it affects scaling behavior even on the one-particle level [1 – 3] — is not renormalized with decreasing the electron density and does not have a strong effect on transport processes. The electron – phonon interaction is also negligible in the low-temperature range $T \ll T_F$, especially for a monatomic crystal such as Si, in which the electron – phonon coupling is only via the deformation potential, with no piezoelectric component. Therefore, by the method of exclusion, the only interaction left to consider is the electron – electron (e – e) interaction.

In this case, it becomes clear where the high value of the carrier mobility μ comes into play. According to the Ioffe – Regel criterion, electrons become localized when their Fermi wavelength becomes equal to the mean free path, $\lambda_F \approx l_{tr}$. Hence, at the localization threshold, the Fermi energy is inversely proportional to the carrier mobility μ: $E_F \propto 1/\tau_{tr} \propto 1/\mu$. We note that for a 2D system, the Fermi energy is proportional to the electron concentration, $E_F \propto n$. It then follows that the higher the mobility (purity) in the 2D system, the lower the electron density that can be achieved in the 'metallic' phase and the stronger the electron – electron interaction, which is usually characterized by the dimensionless ratio of the Coulomb potential energy E_{ee} to the Fermi kinetic energy E_F,

$$r_s = \frac{E_{ee}}{E_F} = \frac{e^2 2m}{\varkappa \pi^{1/2} \hbar^2 n^{1/2}} \propto n^{-1/2}\,.$$

In the relevant experiments, the critical values of the density n_c corresponded to the value $r_s \approx 10$, making it obvious that such a system is by no means an ideal Fermi gas.

Realizing the importance of the electron–electron interaction led to the intense theoretical and experimental studies of its role in 2D systems in recent years. Experimental studies were made of the e–e interaction-induced renormalization of the parameters such as the g-factor $g^*/g = 1/(1 + F_0^a)$, the effective mass $m^*/m = 1 + F_1^s/2$, the compressibility $\varkappa^*/\varkappa = (m^*/m)/(1 + F_0^s)$, and the spin susceptibility $\chi^*/\chi = (m^*/m)/(1 + F_0^a)$. Here, g, m, $\varkappa$, and χ are the corresponding bare (band) values, and $F_i^{a(s)}$ is the lowest-order, antisymmetric (symmetric) Fermi-liquid constant.

Different groups used different experimental techniques to measure the spin susceptibility and effective mass renormalization [22–37] (for brief reviews, see Refs [20, 21]). Figure 2a shows the results of two independent measurements of χ^* for 2D electrons in Si-MOS structures [22, 23] and a GaAs/AlGaAs heterojunction [24]. As one can see, the results are in quite good agreement despite the difference in the carrier effective mass between Si and GaAs by a factor of three, the difference in the 'thickness' of the 2D layer by a factor of six, and the difference in the character and amount of disorder between samples prepared by different techniques. The dependence $\chi^*(r_s)$ turns out to be universal for samples of the same type with different disorder: for example, for Si-MOS structures, there is good agreement in results for samples with different mobilities [20, 23].

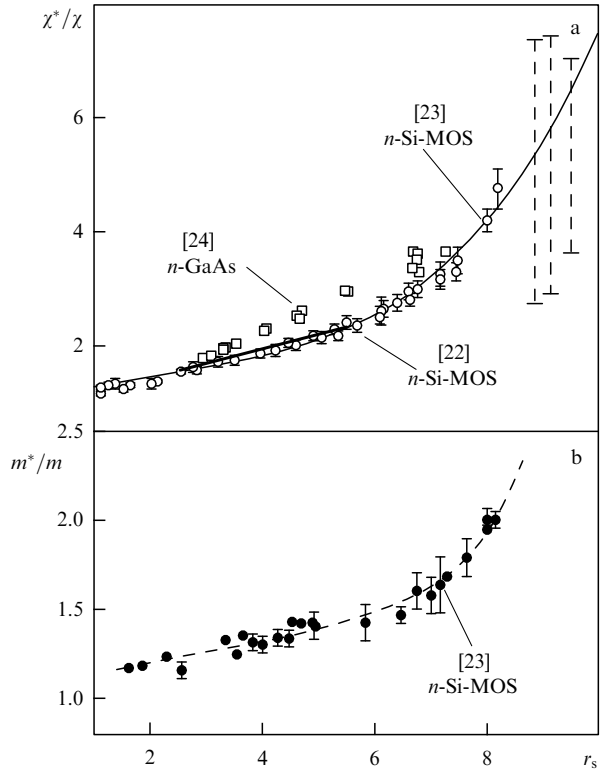

Figure 2. Renormalized spin susceptibility (a) and renormalized mass (b) as measured from Shubnikov–de Haas oscillations. White and black circles: measurements in Si-MOS structures in crossed fields [23], straight solid line: Si-MOS in a tilted field [22], squares: n-GaAs [24]. Horizontal bars on vertical dashed straight lines indicate the upper and lower estimates for χ^* as obtained from the period and phase of Shubnikov–de Haas oscillations [20].

Experimental determination of the renormalized effective mass renormalization is a more difficult task experimentally because it requires a detailed theory. While the experiments on Si-MOS structures all suggest a strong mass renormalization, there is only qualitative agreement among them [20]. One explanation for the quantitative spread is disagreement between the models the researchers used to extract the effective mass from the experimental data. It is also possible that the effective mass renormalization is different in different effects — in kinetics and thermodynamics, for example. Finally, the effective mass may be strongly temperature-dependent, and hence measurements in different temperature ranges may lead to different results.

The first major result from the experimental study of the renormalized parameters of 2D electrons was that, based on the measured values of renormalized parameters and using theoretical predictions for quantum interaction corrections [38, 39], it allowed a satisfactorily qualitative (and, in some cases, even quantitative) description of a) the 'metallic' temperature dependence of conductivity in the absence of a field and b) magnetoresistivity in a parallel magnetic field [25–28, 40]. Figure 3 gives an example of how the measured dependences $\sigma(T)$ compare with the calculated quantum interaction corrections [28]. It can be seen that over a wide range of electron densities (but for $n \gg n_c$), the agreement between theory and experiment is good if one uses the renormalized parameters $g^*(n)$ and $m^*(n)$ measured in independent experiments [23].

To summarize, the metallic temperature dependence of conductivity is now well understood — at least away from the transition, for $\sigma \gg e^2/h$, $n \gg n_c$, and $T \ll T_F$ — and is primarily determined by corrections in the triplet channel of the e–e interaction, which increase with decreasing the density. For the two-valley system of carriers in a Si-MOS

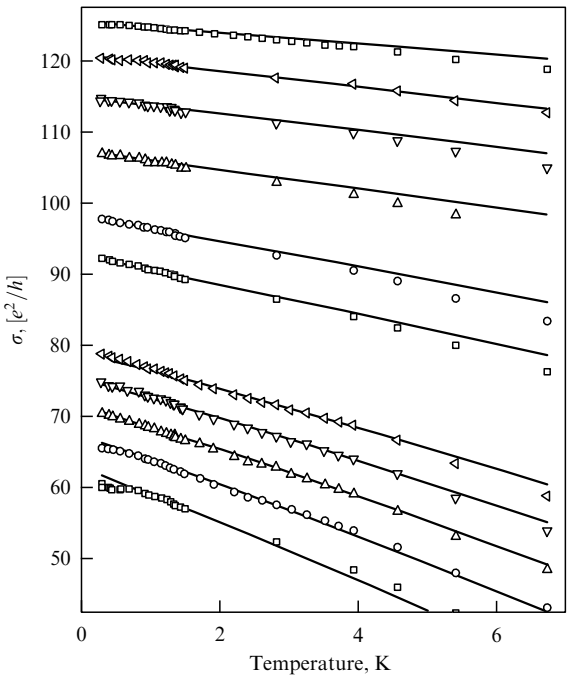

Figure 3. Comparison of the measured temperature dependence of conductivity [28] for the Si-MOS structure Si-22 (symbols) with predicted first-order corrections (solid curves) [38]. Concentrations (from top down) are 21.3, 18.9, 16.5, 14.1, 11.7, 10.5, 8.1, 7.5, 6.9, 6.3 (in units of 10^{11} cm^{-2}).

structure, the number of triplet terms increases by a factor of five [41] — explaining why the metallic behavior of conductivity is that strong in Si structures. But this picture cannot be extended to the critical regime of small $\sigma \sim e^2/h$ (i.e., $k_F l \sim 1$) near the transition ($n \approx n_c$), where the theory of quantum corrections is invalid.

Another major experimental result is that the renormalized parameters are very much the same, whether measured at the Fermi level from Shubnikov – de Haas oscillations [22 – 24] or, alternatively, over a wider energy range from spin polarization [31] or from magnetoresistance scaling in a strong magnetic field [30]. This implies that the interaction of 2D electrons in the strongly correlated regime is not sensitive to the Zeeman energy, i.e., that it occurs via spinless excitations over a wide energy range rather than in the narrow $k_B T$-neighborhood of the Fermi energy (which, we note, is exactly the kind of interaction typical of bosons). Fully consistently with this experimental fact, Iordanskii and Kashuba [42] considered a 2D system of fermions in the limit case of an infinite number of valleys, $n_v \to \infty$. In this approximation, the exchange occurs via high-energy plasmons, leading to the renormalization of the polaron-type effective mass and of the spin susceptibility; we note that the g-factor remains unchanged in the process.

A third key finding is that χ^* increases dramatically (by a factor of five or more) with decreasing density (see Fig. 2). In some papers, this increase was interpreted as a signature of the developing spontaneous spin polarization. If that were the case, the metal – insulator transition might result from a spontaneous ferro- or antiferromagnetic transition.

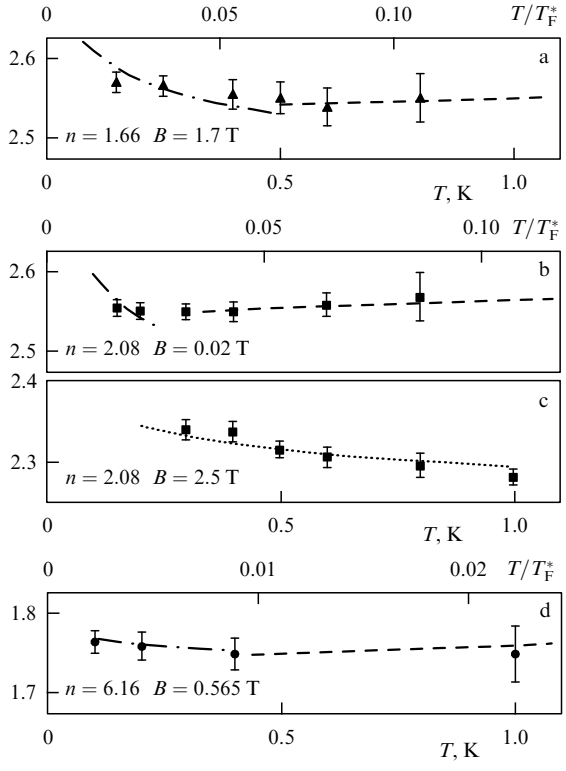

Figure 4. Temperature dependence of χ^* for three values of concentration (shown in units of 10^{11} cm^{-2}) for samples Si6-14 (a – c) and Si3-10 (d) [43]. Upper abscissa scales show temperature in units of the renormalized Fermi energy. Dot-dashed lines are the calculated quantum corrections in the diffusive regime [1], dashed lines are the same for the ballistic regime.

This intriguing possibility — the occurrence of a spontaneous magnetic transition — was tested in Ref. [20] by analyzing the frequency and phase of Shubnikov – de Haas oscillations at low densities. It was found that the frequency of the oscillations does not double until the very moment of the metal – insulator transition, thereby not confirming the doubling of the Fermi energy, which inevitably results from a spontaneous transition of electrons to one spin band. The analysis of the oscillation phase in the same study [20] also shows that the spin splitting in a weak field is more than half of the full cyclotron splitting but does not exceed it — an experimental fact that imposes the upper and lower limits of the spin susceptibility, as shown in Fig. 2a by the short horizontal bars.

In principle, the spin susceptibility could diverge in accordance with a power law with decreasing temperature, signaling the non-Fermi-liquid behavior of a strongly correlated 2D system. This possibility was examined by measuring the temperature variation of spin susceptibility in Refs [20, 43]. Typical $\chi^*(T)$ curves are shown in Fig. 4, which demonstrates that the temperature dependence of the susceptibility is much slower than a power law and is in qualitative agreement with the calculated quantum interaction corrections [1] $\propto \ln T\tau$ for $T\tau \ll \hbar$. We note that taken together, the data above and those from other experiments have not yet revealed any deviations from the Fermi-liquid theory.

3. Interplay of disorder and interaction

The theory of quantum corrections is not applicable near n_c, where $\sigma \sim e^2/h$. In the presence of impurities, fluctuations in local charge, spin, and valley densities show a decay on large length scales, which is equivalent to the propagation of paired electron – hole and electron – electron modes known as diffusons and cooperons [1, 2, 44]. Diffusing electrons become 'more correlated' after spending much time close to each other, which leads to disorder-dependent corrections to the interaction amplitudes $\gamma_2 = F_0^a/(1 + F_0^a)$ and γ_c that characterize the scattering of the diffuson and cooperon modes [44]. In a 2D system, all these corrections diverge logarithmically as temperature decreases [1, 2].

In the 1980s, a technique for resummation of logarithmically divergent diagrams (in fact, an extension of the nonlinear sigma-model) was developed by Finkel'stein [44] and subsequently by Castellani and Di Castro [45, 46], which starts from a weakly interacting system and allows approaching the strong-coupling regime corresponding to the metal – insulator transition. It turns out that even in the lowest-order small-resistance (small-disorder) approximation, the temperature diagram calculated in Ref. [41] (Fig. 5) in terms of the temperature logarithm versus disorder (i.e., resistance) is in qualitative agreement with the observed $\rho(T)$ behavior [16] in the critical regime. As the temperature decreases, the resistivity first increases and then, in accordance with the theory, its behavior starts to be determined by the developing renormalization of γ_2 — with the result that the resistivity passes a maximum and starts decreasing.

In the corresponding two-parameter scaling theory [41, 44 – 47], the renormalization of disorder with decreasing temperature (the increase in the quantum length scale) leads to an increase in interaction, which in turn affects the resistivity (disorder). Therefore, the metal – insulator transi-

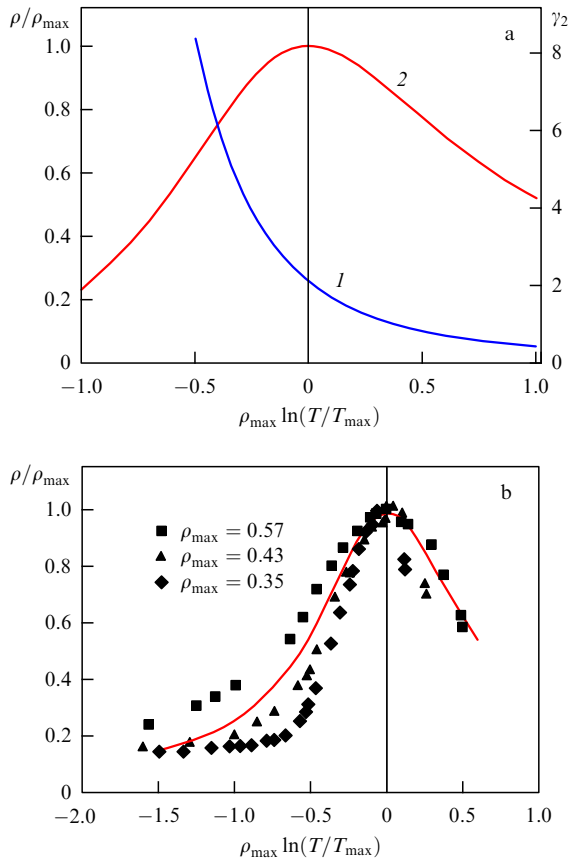

Figure 5. (a) Phase diagram for two-parameter scaling in the one-loop approximation [41]. The abscissa is proportional to the length scale (temperature logarithm), the ordinate is the resistance (disorder) normalized to the maximum value ρ. Curve *1* corresponds to the coupling constant γ_2 in the triplet channel; curve *2*, to resistance. (b) Experimental data from Ref. [16] on $\rho(T)$ (symbols) for three values of concentration are compared with the solution of the renormalization-group equation for a two-valley system [41] (solid curve). The $\rho(T)$ data are normalized by the corresponding maximum values [41].

tion occurs not as a result of the competition between dimensionality and interference (as in the 3D case) but because of the competition between disorder and interaction. Similarly to the theory of quantum corrections [38], the large number (15) of the triplet terms in a two-valley system that facilitate delocalization greatly increases the chances of the system for delocalization compared with those of a one-valley system.

Even though there is qualitative similarity between the theoretical and observed behavior of the resistivity $\rho(T)$, so far experiments have not yet supported the theoretical prediction of a strong increase in γ_2 — demonstrating only a slight variation in the susceptibility with temperature instead (see Fig. 4). A possible reason for this is that the temperature variation of the susceptibility (see Fig. 3) was probably measured not in the critical regime $n \approx n_c$ but for $n \geqslant 1.3n_c$ and in a finite magnetic field; we note that it is not yet possible experimentally to measure susceptibility in a weak field $H < T/g\mu_B$, $H < \pi T/eD$ (D is the diffusion coefficient) [1], as needed for a strict comparison with theory [17].

The result in Ref. [41] derived in the lowest order in resistivity only shows the 'metallization' trend in a 2D system and is not applicable near the transition, where the change in the resistivity with temperature is not minor. Nor does this result apply at the temperature at which γ_2 diverges, and even though this temperature is vanishingly low, $\sim \exp(-\exp((2n_v)^2))$ Kelvin [47], the failure of the scaling equations at sufficiently low temperatures is a drawback of this approximation [41].

Recently, Punnoose and Finkel'stein [47] used the approximation of an infinite number of valleys $n_v = \infty$ in Ref. [42] to obtain a two-loop solution of the renormalization group equations and to show the existence of a quantum critical repulsive point for a metal–insulator transition in the phase diagram of an interacting 2D system. Figure 6 shows a fragment of a phase diagram in Ref. [47], where the repulsive point is shown as a white circle and the arrows indicate the direction of flow as the temperature decreases. Seen in the figure are two classes of trajectories above and below the critical point, which correspond to the insulator and metal, respectively. The dashed line that starts almost horizontally from high temperatures (zero on the abscissa axis) is the separatrix between the metallic phase (bottom left) and the insulator (top left). The second separatrix [the one falling to the point (0, 1)] and the two other phases (top right and bottom right) that it separates have not yet been seen experimentally and may be due to the approximation used ($n_v = \infty$). Varying disorder (for example, the collision frequency $1/\tau$) at a fixed temperature results in motion along a vertical trajectory that intersects the separatrix (shown dashed in Fig. 6), thus leading to a metal–insulator quantum transition. Treating the electron concentration as a parameter implies a simultaneous variation of the bare disorder and bare interaction r_s, such that the system undergoes a metal–insulator transition again, but with the difference this time that it goes along a tilted rather than vertical trajectory when intersecting the separatrix.

In the limit as $T \to 0$, the flow lines in Fig. 6 converge to a point corresponding to an ideal metal, seemingly violating the Fermi-liquid picture [4, 48]. But it is reasonable to expect that when the system is cooled such that T becomes less than both $\hbar/\tau_s$ and $\hbar/\tau_{vv}$ (where τ_s and τ_{vv} are the spin flip and intervalley scattering times, respectively), the contribution of the triplet (delocalizing) terms sharply diminishes, restoring the singlet-to-triplet ratio common for a single-component Fermi liquid [1, 2]. The corresponding cut-off temperatures depend on the parameters of the scatterers present in the

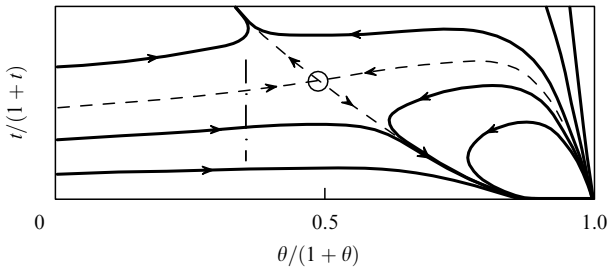

Figure 6. Phase diagram of two-parametric scaling in the approximation of an infinite number of valleys [47]. The vertical and horizontal axes represent the disorder t ($t = 1/(2\pi)^2 vD$, resistivity per valley) and interaction θ, respectively. Arrows indicate where the data point moves as the temperature decreases. The circle depicts the quantum critical repulsive point. Shown dashed is the separatrix between the metallic and insulating phases. Vertical dash-dot line depicts an order-changing trajectory for the metal–insulator transition at the temperature chosen.

sample. By way of estimate, we note that $\hbar/\tau_s \sim 10^{-6}$ K; the experimental data on $\hbar/\tau_{vv}$ in the range from 10^{-1} to 10^{-4} K are as yet of low reliability. This question is purely academic, however, because such low temperatures are many orders of magnitude below the currently accessible level.

In summary, theory suggests an extraordinary picture, where the metal–insulator transition occurs at a finite temperature and is a true quantum transition, but, strictly speaking, the metallic state that results does not survive the $T = 0$ limit (provided the 2D system does not make a spontaneous transition to another universality class — due to the formation of local magnetic moments [48] or of a two-phase microemulsion state [49], for example). Other remaining questions are whether the phase diagram of a 2D metal–insulator transition will be valid, at least in general terms, for realistic cases such as $n_v = 6$, 2 or 1, and down to what temperatures a 2D metal can exist in real-life systems.

Acknowledgements The above experimental study by the present author and coworkers was supported by grants from the RFBR, INTAS, RAS Presidium programs, RAS Physics Sciences Division programs, and the President's program for leading scientific schools.

References

1. Al'tshuler B L, Aronov A G, in *Electron-Electron Interactions in Disordered Systems* (Modern Problems in Condensed Matter Sciences, Vol. 10, Eds A L Efros, M Pollak) (Amsterdam: North-Holland, 1985) p. 1
2. Lee P A, Ramakrishnan T V *Rev. Mod. Phys.* **57** 287 (1985)
3. Altshuler B L, Aronov A G, Khmelnitskii D E, Larkin A I, in *Kvantovaya Teoriya Tverdogo Tela* (Quantum Theory of Solids) (Ed. I M Lifshits) (Moscow: Mir, 1982) [Translated into English (Moscow: Mir Publ., 1982) p. 130]
4. Abrahams E et al. *Phys. Rev. Lett.* **42** 673 (1979)
5. Wigner E *Phys. Rev.* **46** 1002 (1934)
6. Tanatar B, Ceperley D M *Phys. Rev. B* **39** 5005 (1989)
7. Chui S T (Ed.) *Physics of 2D Quantum Electron Solids* (Cambridge, MA: International Press, 1994)
8. D'Iorio M, Pudalov V M, Semenchinsky S G *Phys. Lett. A* **150** 422 (1990)
9. D'Iorio M, Pudalov V M, Semenchinsky S G *Phys. Rev. B* **46** 15992 (1992)
10. Pudalov V M, D'Iorio M, Campbell J W *Pis'ma Zh. Eksp. Teor. Fiz.* **57** 592 (1993) [*JETP Lett.* **57** 608 (1993)]
11. Kravchenko S V et al. *Phys. Rev. Lett.* **75** 910 (1995)
12. Khmelnitskii D E *Phys. Lett. A* **106** 182 (1984)
13. Laughlin R B *Phys. Rev. Lett.* **52** 2304 (1984)
14. Kravchenko S V et al. *Phys. Rev. B* **50** 8039 (1994)
15. Kravchenko S V et al. *Phys. Rev. B* **51** 7038 (1995)
16. Pudalov V M et al. *Pis'ma Zh. Eksp. Teor. Fiz.* **68** 415 (1998) [*JETP Lett.* **68** 442 (1998)]; *Physica E* **3** 79 (1998)
17. Pudalov V M, in *The Electron Liquid Paradigm in Condensed Matter Physics* (Proc. of the Intern. School of Physics Enrico Fermi, Course CLVII, Eds G F Giuliani, G Vignale) (Amsterdam: IOS Press, 2004) p. 335; cond-mat/0405315
18. Abrahams E, Kravchenko S V, Sarachik M P *Rev. Mod. Phys.* **73** 251 (2001)
19. Altshuler B L, Maslov D L, Pudalov V M *Physica E* **9** 209 (2001)
20. Pudalov V M, Gershenson M, Kojima H, in *Fundamental Problems of Mesoscopic Physics*: *Interactions and Decoherence* (NATO Sci. Ser., Ser. II, Vol. 154, Eds I V Lerner, B L Altshuler, Y Gefen) (Dordrecht: Kluwer Acad. Publ., 2004) Ch. 19, p. 309
21. Shashkin A A *Usp. Fiz. Nauk* **175** 139 (2005) [*Phys. Usp.* **48** 129 (2005)]
22. Okamoto T et al. *Phys. Rev. Lett.* **82** 3875 (1999)
23. Pudalov V M et al. *Phys. Rev. Lett.* **88** 196404 (2002)
24. Zhu J et al. *Phys. Rev. Lett.* **90** 056805 (2003)
25. Proskuryakov Y Y et al. *Phys. Rev. Lett.* **89** 076406 (2002)
26. Shashkin A A et al. *Phys. Rev. B* **66** 073303 (2002)
27. Vitkalov S A et al. *Phys. Rev. B* **67** 113310 (2003)
28. Pudalov V M et al. *Phys. Rev. Lett.* **91** 126403 (2003); *Phys. Rev. Lett.* **93** 269704 (2004)
29. Vitkalov S A et al. *Phys. Rev. Lett.* **87** 086401 (2001)
30. Shashkin A A et al. *Phys. Rev. Lett.* **87** 086801 (2001)
31. Vitkalov S A, Sarachik M P, Klapwijk T M *Phys. Rev. B* **65** 201106 (2002)
32. Yoon J et al. *Phys. Rev. Lett.* **84** 4421 (2000)
33. Tutuc E et al. *Phys. Rev. Lett.* **86** 2858 (2001)
34. Tutuc E et al. *Phys. Rev. B* **67** 241309(R) (2003)
35. Tutuc E, Melinte S, Shayegan M *Phys. Rev. Lett.* **88** 036805 (2002)
36. Pudalov V M et al. *Phys. Rev. Lett.* **88** 076401 (2002)
37. Prus O et al. *Phys. Rev. B* **67** 205407 (2003)
38. Zala G, Narozhny B N, Aleiner I L *Phys. Rev. B* **64** 214204; **65** 020201 (2001)
39. Gornyi I V, Mirlin A D *Phys. Rev. B* **69** 045313 (2004)
40. Olshanetsky E B et al. *Phys. Rev. B* **68** 085304 (2003)
41. Punnoose A, Finkel'stein A M *Phys. Rev. Lett.* **88** 16802 (2002)
42. Iordanski S V, Kashuba A *Pis'ma Zh. Eksp. Teor. Fiz.* **76** 660 (2002) [*JETP Lett.* **76** 563 (2002)]
43. Pudalov V M et al. *Phys. Rev. B* (to be published)
44. Finkel'shtein A M *Zh. Eksp. Teor. Fiz.* **84** 168 (1983); **86** 367 (1984) [*Sov. Phys. JETP* **57** 97 (1983); **59** 212 (1984)]; Finkel'stein A M *Z. Phys. B* **56** 189 (1984); *Sov. Sci. Rev. Sect. A Phys. Rev.* (Ed. I M Khalatnikov) **14** (2) 3 (1990)
45. Castellani C et al. *Phys. Rev. B* **30** 527 (1984)
46. Castellani C et al. *Phys. Rev. B* **30** 1596 (1984)
47. Punnoose A, Finkel'stein A M *Science* **310** 289 (2005)
48. Dobrosavljević V et al. *Phys. Rev. Lett.* **79** 455 (1997)
49. Spivak B, Kivelson S A *Phys. Rev. B* **70** 155114 (2004)

PACS numbers: 71.10.Ca, **71.27 + a**, 73.43.Cd
DOI: 10.1070/PU2006v049n02ABEH005922

Two-dimensional multicomponent electron gas as a model for silicon heterostructures

S V Iordanskii, A Kashuba

1. Introduction

Two-dimensional electron gas in a Si-heterostructure can vary very widely in density [1]. Effects due to the electron–electron Coulomb interaction are determined by the dimensionless ratio of the average Coulomb energy to the electron kinetic energy, $r_s = e^2 m/\sqrt{\pi n}\,\hbar^2$, with n being the electron density. For relatively large r_s, $1 < r_s < 10$, Si-MOSFETs (metal-oxide-semiconductor field-effect transistors) undergo a transition from the metallic (growing) to dielectric (falling) conductivity with decreasing temperature [2] and demonstrate an increase in the effective mass and magnetic susceptibility with increasing r_s [3, 4]. Because of the lack of exactly solvable models for large r_s, various phenomenological models have come to the fore. The electron–hole plasma observed in a three-dimensional (3D) electron–hole droplet in Si and Ge is also characterized by comparatively large values of r_s. As shown in the pioneering work of Ref. [5], the multivalley band structure leads to the existence in these semiconductors of a 'metallized' electron–hole plasma in the region of relatively large r_s (see also Ref. [6]). One would expect that allowing for many valleys in two-dimensional (2D) Si-heterostructures would lead to better agreement with experiment compared with Landau's Fermi-liquid theory with its small-r_s corrections to the theory of a dense electron gas. The Fermi-liquid theory predictions for Si-heterostructures are in quantitative disagreement with experiment even

at moderate values of r_s. For example, the theory of a dense electron gas predicts an increase in the effective mass at small r_s, [7],

$$\frac{m^*}{m} = 1 - \frac{r_s}{\pi} \log\left(\frac{1}{r_s}\right), \tag{1}$$

whereas Shubnikov – de Haas measurements [8, 9] yield

$$\frac{m^*}{m} \approx 1 + 0.08 r_s \,. \tag{2}$$

Another point to note concerns charged excitations on the lowest filled Landau level. Experimentally, their activation energy (which is small according to the magnetoconductance measurements in Ref. [10]) is roughly proportional to the magnetic field H, whereas theoretically [11], it must be proportional to its square root, $e^2\sqrt{eH/\hbar c}$ (the same as the electron – electron interaction). These phenomena are observed at $1.5 < r_s < 3$, which is far from the metal – insulator transition. We show that a systematic model of a 2D multicomponent high-density electron gas gives qualitative agreement with the experimental data for highest-purity silicon heterostructures.

Electron states in silicon have valley degeneracy [1] that corresponds to different band energy maxima. For the (1,0,0)-oriented heterostructure plane in a silicon crystal, there are $N = 4$ equivalent, orthogonal spin-valley electron states that differ by a factor $\exp(\pm \mathrm{i} Q z)$ in the perpendicular direction with atomic wave vector Q. For the $(1, 1, 1)$ orientation, the spin-valley degeneracy is $N = 12$. A 3D electron gas in the limit $N \to \infty$ was first treated in Ref. [12].

2. Multicomponent Fermi liquid

A systematic theory can be developed in the limit $1 > r_s \gg N^{-3/2}$, where it differs quite substantially from the $r_s \ll N^{-3/2}$ limit theory, which yields standard Fermi-liquid results. The model is described by the Hamiltonian

$$\hat{H} = \frac{1}{2m} \int \psi_\alpha^\dagger(\mathbf{r}) \left(-\mathrm{i}\hbar\nabla + \frac{e}{c}\,\mathbf{A}(\mathbf{r}) \right)^2 \psi_\alpha(\mathbf{r})\, \mathrm{d}^2\mathbf{r} + \frac{1}{2} \iint \frac{e^2}{|\mathbf{x} - \mathbf{r}|}\, \psi_\alpha^\dagger(\mathbf{x})\, \psi_\beta^\dagger(\mathbf{r})\, \psi_\beta(\mathbf{r})\, \psi_\alpha(\mathbf{x})\, \mathrm{d}^2\mathbf{x}\, \mathrm{d}^2\mathbf{r} \,, \tag{3}$$

where valley-to-valley transitions are not allowed, α and β are conserved ($\alpha, \beta \leqslant N$) as in the exchange approximation, and the mass m is isotropic. It is assumed that there is a compensating positive charge at a large distance from the heterostructure plane. The summation is over the spin-valley indices.

The effect of a multivalley structure primarily shows up as a highly screened Coulomb interaction. The Coulomb interaction gives rise to polarization effects in each valley, thus decreasing interaction between electrons residing in the same valley. Accordingly, even though $r_s^{(1)}$ calculated only for the electrons in one valley may be large, $r_s(N)$ for all the N valleys is small, enabling expressions for physical properties to be systematically expanded in powers of $r_s(N)$. For our purposes, the Matsubara diagram technique as applied in its low-temperature limit [13] is sufficient. In the 2D limit (i.e., at distances much longer than the heterostructure thickness), the Coulomb interaction between electrons in the heterostructure has the Fourier component

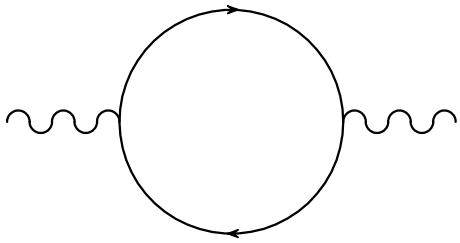

Figure 1. Polarization bubble. Electron propagators and the Coulomb interaction are represented by arrowed and wavy lines, respectively.

$$V(\mathbf{q}) = \frac{2\pi e^2}{|\mathbf{q}|} \,. \tag{4}$$

Calculating the effective interaction requires knowing the electron polarization by the interaction field in all the valleys, which can be depicted by the diagram in Fig. 1, showing the creation of electron – hole pairs by the Coulomb interaction. In this figure, the normal line represents the free electron Green's function

$$G_\alpha^0(\varepsilon, \mathbf{p}) = \frac{1}{\mathrm{i}\varepsilon - (\varepsilon_\alpha(\mathbf{p}) - \mu)} \,, \tag{5}$$

where $\varepsilon(\mathbf{p}) = p^2/2m$ is spin- and valley-independent, and the wavy line is for the Fourier component of Coulomb interaction (4). The calculation of the effective interaction involves summation over all valleys and requires that the polarization effects of all orders be included. This means using the random-phase approximation (RPA) and summing all diagrams with the number of polarization bubbles being maximum for a given number of interaction lines:

$$V_{\mathrm{eff}}(\omega, q) = \frac{2\pi e^2/q}{1 + (2\pi e^2/q)\, \Pi(\omega, q)} \,, \tag{6}$$

where $\Pi(\omega, q)$ corresponds to the diagrams for a single polarization bubble. Because the one-valley electron density n_1 is small compared with the total density $n = N n_1$, the Fermi momentum p_F is also small compared with the momentum transfer q. In the limit $q \gg p_F$, the quantity $\Pi(\omega, q)$ is easily calculated to be

$$\Pi(\omega, q) = \frac{2n\varepsilon(q)}{\omega^2 + \varepsilon^2(q)} \,, \tag{7}$$

and the effective Coulomb interaction becomes

$$D(\omega, q) = \frac{2\pi e^2}{q}\, \frac{\omega^2 + \varepsilon^2(q)}{\omega^2 + \varepsilon^2(q) + 4\pi e^2 n \varepsilon(q)/q} \,. \tag{8}$$

The poles of $D(\omega, q)$ correspond to zeros of the dielectric constant and yield the plasmon excitation energy

$$\omega(q) = \frac{\hbar^2}{2m} \sqrt{q^2 + q_0^3 q} \,, \tag{9}$$

where $q_0^3 = 8\pi e^2 n m/\hbar^2$ is the characteristic momentum of the effective interaction. Thus, the plasmon energy turns out to be large compared to the kinetic energy ε_F, making the effective interaction small.

Diagram calculations can be interpreted in terms of a picture in which plasmons, described by the propagator $D(\omega, q)$, interact with one another via closed loops containing more than two electron lines. A vertex containing $k > 2$ plasmon lines with large momenta $\sim q_0$ and with frequencies $\omega_0 \sim q_0^2/2m$ is of the order of $V_k \sim n/\omega_0^{k-1}$. With these estimates, it is possible to classify all the diagrams by powers of $r_s^{2/3}$. The correlation energy per unit volume calculated in the next-to-leading order is given by

$$E_c = -\left(2.03191\ r_s^{4/3} - 0.156(1)\ r_s^2\right)\ \frac{n^2}{m}\,. \tag{10}$$

But it is more interesting to calculate corrections to the electron Green's function

$$G^{-1}(\varepsilon, \mathbf{p}) = \mathrm{i}\varepsilon - \left(\varepsilon(\mathbf{p}) - \mu\right) - \Sigma(\varepsilon, \mathbf{p})\,. \tag{11}$$

Because of the small magnitude of the screened interaction, the mass operator may be calculated in the first order in the plasmon operator $D(\omega, q)$,

$$\Sigma(\varepsilon, \mathbf{p}) = -\int D(\omega, \mathbf{q})\, G(\varepsilon + \omega, \mathbf{p} + \mathbf{q})\ \frac{\mathrm{d}\omega\, \mathrm{d}^2\mathbf{q}}{(2\pi)^3}\,. \tag{12}$$

Because of the large values of the plasmon momentum and energy, the integral can be evaluated by taking $\varepsilon \ll \omega$ and $p \ll q$, and the Green's function near the Fermi surface takes the form

$$G(\varepsilon, p) = \frac{Z(p_F)}{\mathrm{i}\varepsilon - \varepsilon_R(p) + \mu}\,, \quad \varepsilon_R(p) = \frac{p_F}{m^*}\,(p - p_F)\,, \tag{13}$$

where, for small r_s,

$$\frac{m}{m^*} = 1 - \frac{1}{10\sqrt{\pi}}\ \Gamma\left(\frac{1}{3}\right)\Gamma\left(\frac{7}{6}\right)\ r_s^{2/3} + O(r_s^{4/3})\,,$$

$$Z^{-1}(p_F) = 1 + \frac{1}{2\sqrt{\pi}}\ \Gamma\left(\frac{1}{3}\right)\ \Gamma\left(\frac{7}{6}\right)\ r_s^{2/3} + O(r_s^{4/3})\,, \tag{14}$$

where $\Gamma(v)$ is the gamma function.

Similarly, for the spin magnetic susceptibility, we obtain

$$\frac{\chi^*}{\chi} = \frac{m^*}{m}\,, \tag{15}$$

where $\chi = m/2\pi\hbar^2$ is the susceptibility of a 2D Fermi gas of Pauli. Figure 2 compares experimental data on m^*/m and χ^*/χ [14] with theoretical predictions. It can be seen that the effective mass shows good agreement, whereas the susceptibility is somewhat underpredicted — due to exchange effects, which are absent in the theory at $N = \infty$ but should show up in real silicon at $N = 4$. (We also note that at $r_s \approx 9$, a Si-MOSFET undergoes a metal–insulator transition, which is beyond our theoretical model).

We note that the effective mass and magnetic susceptibility renormalization in Landau's Fermi liquid theory are related to the properties of the (scattering-angle-dependent) effective interaction function of the particles involved [15]. Unlike this, in a multicomponent gas, these Fermi-liquid parameters are determined by the properties of plasmons, whose energies and momenta are much larger than those of the Fermi-surface electrons. Besides, the small Fermi momentum together with strong screening effects prevents Friedel density oscillations from occurring in a multicomponent gas.

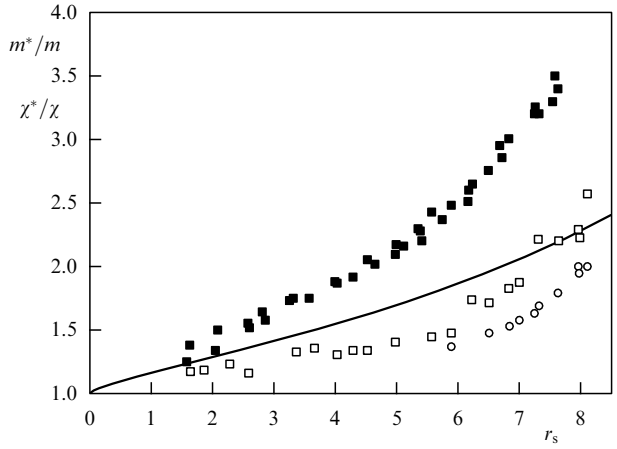

Figure 2. Experimental data for the magnetic susceptibility χ^*/χ (black squares) and effective mass m^*/m (white circles and squares). Solid curve: the susceptibility and mass obtained from the multicomponent model.

To show this, we note that the induced charged density in a multicomponent gas is given by

$$\delta n(\mathbf{r}) = \int \frac{2\pi e^2 \Pi(0, q)}{q + 2\pi e^2 \Pi(0, q)}\ \exp(\mathrm{i}\mathbf{q}\mathbf{r})\ \frac{\mathrm{d}^2\mathbf{q}}{(2\pi)^2}$$

$$= \int_0^\infty \frac{q_0^3}{q^3 + q_0^3}\ J_0(qr)\ \frac{q\,\mathrm{d}q}{2\pi}\,. \tag{16}$$

The function $\delta n(\mathbf{r})$ is concentrated at $r \sim 1/q_0 \ll 1/p_F$, where it has one zero, and decreases exponentially with distance. The outer charge is fully screened,

$$\int \delta n(\mathbf{r})\, \mathrm{d}^2\mathbf{r} = 1\,. \tag{17}$$

Friedel oscillations [15] are related to the singularity at $q = 2p_F$ [which is neglected in Eqn (7)] and have the period $\pi\hbar/p_F$ and the amplitude $\sim p_F^2/N$, which is vanishingly small in the limit $N \to \infty$. We therefore conclude that many Fermi surface features are absent in a multicomponent gas.

3. Adding a magnetic field

The multicomponent model can be extended to include a large external magnetic field perpendicular to the heterostructure plane. Then the ground state of the system is one with the lowest Landau level filled. We suppose that of N spin-valleys present, only $1 \ll v < N$ have their zeroth level completely filled. Although the system does not make real transitions to higher Landau levels, the virtual transitions it does make screen the Coulomb interaction as before. The unperturbed electron Green's function for one valley can be written as the sum

$$G_0(\varepsilon, \mathbf{r}, \mathbf{r}') = \sum_{s,p} \frac{1}{\mathrm{i}\varepsilon - (s + 1/2)\,\omega_H + \mu}\ \Phi_{sp}(\mathbf{r})\, \Phi_{sp}^*(\mathbf{r}')\,, \tag{18}$$

where s is the Landau index, Φ_{sp} is the Landau-level wave function, and ω_H is the cyclotron frequency. The polarization operator is calculated to be

$$\Pi(\omega, \mathbf{q}) = \frac{v}{2\pi} \sum_{s=1}^{\infty} \frac{q^{2s}}{2^s\ s!}\ \frac{2s\omega_H}{\omega^2 + \omega_H^2 s^2}\ \exp\left(-\frac{q^2}{2}\right), \tag{19}$$

(in a system of units where the magnetic length $l_H = 1$ and $e = c$, $\omega_H = 1/m$). Such a special form of the polarization operator is because the electron – hole polarization loop in the coordinate representation is a function of $(\mathbf{r} - \mathbf{r}')$ if an external magnetic field is present.

A plasmon propagator, like $D(\omega, q)$, has the form (6). In the presence of a completely filled Landau level in $\Pi(\omega, q)$ valleys, additional energy comes into play due to the electron being transferred from an occupied valley to the same level in an empty valley, with a hole left behind. This energy has its origin in exchange effects and corresponds to a spin wave in the one-valley case. This is a neutral excitation, and one which is characterized by a momentum, despite the presence of a magnetic field. In this situation, an exchange exciton forms. At a large momentum, the electron and the hole are far apart, their interaction is negligible, and they can therefore be considered free — leading to the conclusion that their energy is the activation energy for charge excitations, the electron energy difference between the empty and occupied valleys. This energy can be calculated to give

$$\Delta = \int D(0,q)\ \exp\left(-\frac{q^2}{2}\right)\frac{\mathrm{d}^2\mathbf{q}}{(2\pi)^2} = \frac{\hbar\omega_H}{\nu}\left(\log(r_s\nu^{3/2}) + 0.277\right), \qquad (20)$$

($r_s = \sqrt{2}e^2/\omega_H l_H\sqrt{\nu}$), showing that the activation energy is approximately proportional to the magnetic field and is small in the limit of large ν. The linear behavior agrees qualitatively with the magneto-conductance measurements of the activation energy [10], but Eqn (20) greatly overestimates the activation energy — possibly because the extrapolation to relatively large r_s is itself a rather crude procedure or because factors such as a finite thickness of the 2D layer or the image force from the metal gate were not taken into account.

The energy of an exchange exciton at low momentum Q is calculated in a similar way, giving

$$\omega(Q) = J(Ql_H)^2, \quad J = 0.6613\ \frac{\omega_H}{\nu}\,. \qquad (21)$$

Thus, we see that the exchange constant J is also screening-suppressed and varies linearly with the magnetic field.

Some of the results in this paper were previously presented in Ref. [16].

Acknowledgements. This work was supported by RFBR grants 03-02-17229a and 0501-16553a.

References

1. Ando T, Fowler A B, Stern F *Rev. Mod. Phys.* **54** 437 (1982)
2. Abrahams E, Kravchenko S V, Sarachik M P *Rev. Mod. Phys.* **73** 251 (2001)
3. Pudalov V M et al. *Phys. Rev. Lett.* **88** 196404 (2002)
4. Shashkin A A et al. *Phys. Rev. B* **66** 073303 (2002)
5. Bagaev V S et al. *Pis'ma Zh. Eksp. Teor. Fiz.* **10** 309 (1969) [*JETP Lett.* **10** 195 (1969)]
6. Jeffries C D, Keldysh L V (Eds) *Electron-Hole Droplets in Semiconductors* (Modern Problems in Condensed Matter Sciences, Vol. 6) (Amsterdam: North-Holland Publ. Co., 1983)
7. Gell-Mann M, Brueckner K A *Phys. Rev.* **106** 364 (1957); Sawada K *Phys. Rev.* **106** 372 (1957); Gell-Mann M *Phys. Rev.* **106** 369 (1957)
8. Smith J L, Stiles P J *Phys. Rev. Lett.* **29** 102 (1972)
9. Okamoto T et al. *Phys. Rev. Lett.* **82** 3875 (1999)
10. Khrapai V S, Shashkin A A, Dolgopolov V T *Phys. Rev. B* **67** 113305 (2003)
11. Bychkov Yu A, Iordanskii S V, Eliashberg G M *Pis'ma Zh. Eksp. Teor. Fiz.* **33** 152 (1981) [*JETP Lett.* **33** 143 (1981)]; Kallin C, Halperin B I *Phys. Rev. B* **30** 5655 (1984)
12. Takada Y *Phys. Rev. B* **43** 5962 (1991)
13. Abrikosov A A, Gor'kov L P, Dzyaloshinskii I E *Metody Kvantovoi Teorii Polya v Statisticheskoi Fizike* (Methods of Quantum Field Theory in Statistical Physics) (Moscow: Dobrosvet, 1998) [Translated into English (New York: Dover Publ., 1975)]
14. Pudalov V M, Gershenson M E, Kojima H, in *Fundamental Problems of Mesoscopic Physics*: *Interactions and Decoherence* (NATO Sci. Ser., Ser. II, Vol. 154, Eds I V Lerner, B L Altshuler, Y Gefen) (Dordrecht: Kluwer Acad. Publ., 2004)
15. Pines D, Nozières P *The Theory of Quantum Liquids* (New York: W.A. Benjamin, 1966)
16. Iordanski S V, Kashuba A *Pis'ma Zh. Eksp. Teor. Fiz.* **76** 660 (2002) [*JETP Lett.* **76** 563 (2002)]

PACS numbers: **71.27.+a**, **71.30.+h**, 72.15.Rn

DOI: 10.1070/PU2006v049n02ABEH005923

Interaction effects in the transport and magnetotransport of two-dimensional electrons in AlGaAs/GaAs and Si/SiGe heterojunctions

E B Olshanetskii, V Renard, Z D Kvon, I V Gornyi, A I Toropov, J C Portal

1. Introduction

Localization- and interaction-induced quantum corrections to the conductivity of two-dimensional (2D) electron systems [1, 2] have been the subject of considerable study since as long as a quarter century ago. It should be noted that weak localization effects do not present any problems, and that their associated anomalous magnetoresistance very soon became a powerful tool for probing the low-temperature properties of disordered metallic systems, from thin superconducting films to near-surface 2D layers in semiconductors. Unlike this, the behavior of interaction effects remained the subject of continuous heated debate — primarily in connection with how they influence the metal – insulator transition in a 2D electron system [3]. What made things especially topical was the discovery [4] that a high-mobility 2D electron gas in silicon MOS (metal-oxide-semiconductor) transistors exhibits states whose conductivity increases anomalously with lowering the temperature, which is entirely inconsistent with theoretical expectations [1, 2]. This situation has stimulated new ideas in the theory of interaction-induced quantum corrections and has recently led to its further development in Refs [5 – 7], which identified two regimes — the diffusion one (for $T\tau/\hbar \ll 1$) and the ballistic one (for $T\tau/\hbar \gg 1$) — in the behavior of quantum corrections. Both regimes are of the same nature, i.e., are determined by single and multiple scattering from impurities and from the Friedel oscillations in their screening charge. Both mechanisms had already been know before Refs [5 – 7]. The first mechanism [1, 2] was thought to be related to the quantum corrections due to the interference of interacting electrons (see above), and the second was linked to the temperature dependence of screening due to the singularity in 2D screening near $q \approx 2k_F$ [8] and was considered to be a temperature-dependent part of the one-electron transport time, unrelated to quantum interference.

There was a series of experiments [9–12] to verify the predictions in Refs [5–7], and although a number of confirmations were obtained, none of the experiments showed the transition from one regime to the other. Nor was a study done to see experimentally how (or whether) the ballistic and quantum corrections depend on whether the primary scattering mechanism is short-range, long-range, or mixed — even though this had been shown [7] to be a very important factor in determining the behavior of the parabolic magnetoresistance due to these corrections. This talk presents experiments that used 2D electron systems (2D ESs) in an AlGaAs/GaAs/AlGaAs quantum well and in a SiGe/Si heterojunction to clarify the situation.

2. Transition from the ballistic to the diffusion regime in a 2D ES in an AlGaAs/GaAs/AlGaAs quantum well

The experiment to study the way quantum corrections change from diffusion to ballistic behavior involved a specially designed structure consisting of a high-density 2D electron gas (2D EG) in an AlGaAs/GaAs/AlGaAs quantum well doped with Si. With the concentration N_s varying in the range $(2.5-4.5)\times10^{12}$ cm^{-2} and the mobility μ between 280 and 560 cm^2 V^{-1} s^{-1}, the system under study was a low-mobility 2D EG with large values of the Fermi energy E_F ($E_F = 100-200$ meV) and the short-range potential of doped Si atoms acting as the dominant scattering mechanism. To catch the transition from $T\tau/\hbar \ll 1$ to $T\tau/\hbar \gg 1$, the maximum possible temperature range, $T = 1.4-110$ K, was covered, in which the resistance, magnetoresistance, and Hall effect were measured in detail (Fig. 1). Before proceeding to the analysis of the experiment, a close look at the theory in Refs [5, 6] is in order. According to this theory, the total quantum correction to the conductivity of a 2D ES consists of a logarithmic part and a linear part, respectively dominant at low ($T\tau/\hbar \ll 1$) and high ($T\tau/\hbar \gg 1$) temperatures. The point to note here is that in the weak interaction case, $r_s \leqslant 1$ ($r_s = E_{e-e}/E_F$), both corrections have the same sign — one for which the conductivity falls with decreasing the temperature. An interesting prediction concerns the correction $\delta\rho_{xy}$ to the classical Hall resistance ρ_H^D: its temperature dependence changes from logarithmic to hyperbolic as the temperature increases. As already noted, there exists a correction due to weak localization, along with that due to interaction. The former was excluded by conducting experiments in a magnetic field B, which completely suppresses the weak localization in our samples at $B > 5$ T. Another output from measurements in a magnetic field was the value of the Drude conductivity, which is needed for correctly comparing theory and experiment. Measurements of the temperature dependence of conductivity due to the $\Delta\sigma_{xx}^{e-e}(T)$ interaction are presented in Fig. 2a. It is clearly seen that the dependence is close to linear at high temperatures, $T > 20$ K, and becomes logarithmic for $T < 20$ K. A fairly good agreement is seen with the dependence (solid curve) predicted by the theory in Ref. [5]. We note that this agreement is obtained without the use of any fitting parameters because in the weak interaction case, the Fermi-liquid constant F_0^σ, normally used as a fitting parameter, is determined exactly [5] if the

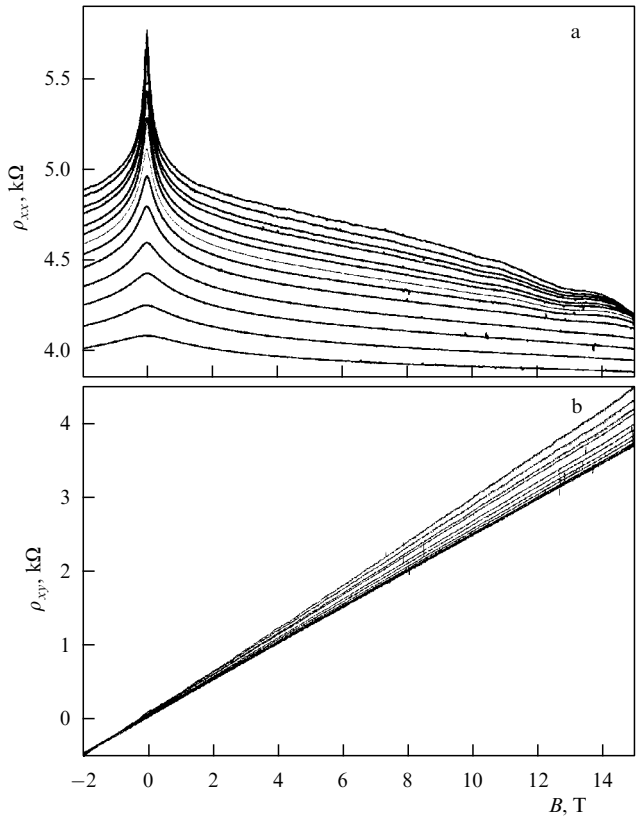

Figure 1. Resistance and magnetoresistance (a) and Hall effect (b) of an AlGaAs/GaAs/AlGaAs quantum well in the temperature range 1.4 K – 110 K.

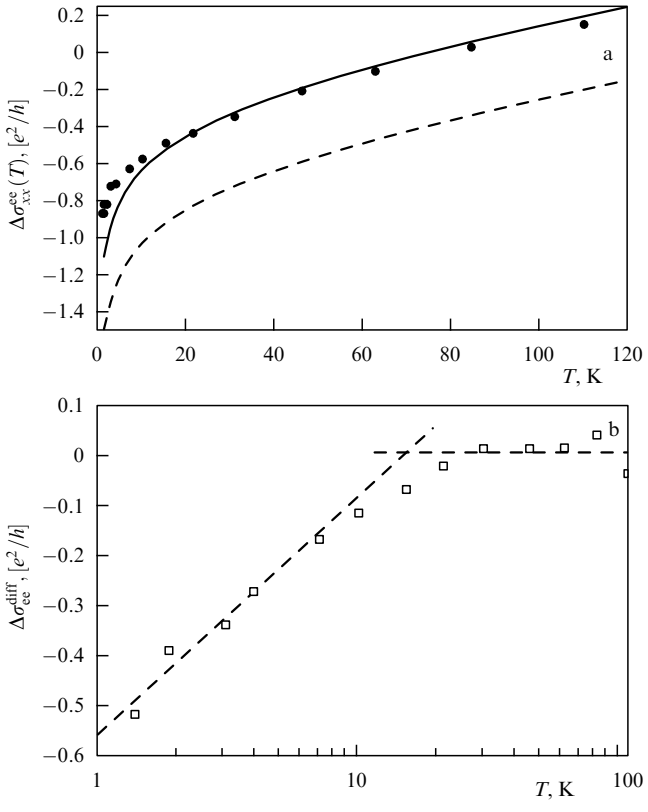

Figure 2. (a) Measured (dots) and calculated (solid line) quantum corrections due to interaction; the dashed line is for the theoretical correction calculated without account for the constant shift. (b) temperature dependence of the logarithmic correction to conductivity.

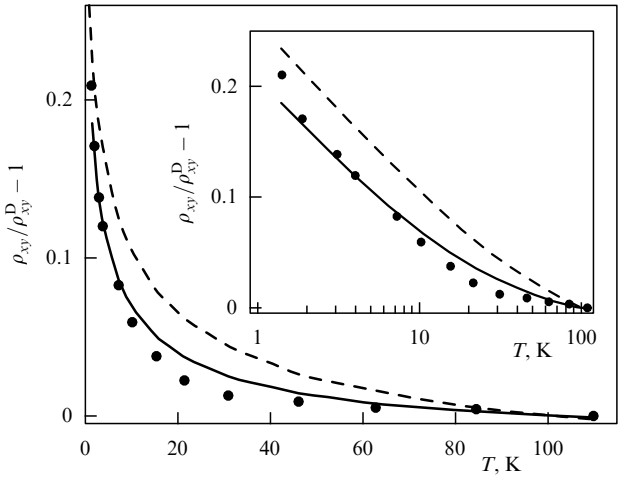

Figure 3. Temperature dependence of the Hall coefficient. Dots: experiment; dashed line: theory in Ref. [6]; solid line: the same for anisotropic electron scattering.

concentration of 2D electrons is known, which in our case was determined which it is from the Hall effect and Shubnikov–de Haas measurements on the samples studied. A specially developed technique allowed each of the interaction-induced corrections to be determined separately. Taking the logarithmic correction as an illustration, it is clearly seen from Fig. 2b that it tends to zero for $T > 20$ K. The measured and predicted corrections to the Hall resistance are compared in Fig. 3, from which it is seen that the theory in Ref. [6] explains the behavior of $\delta\rho_{xy}/\rho_{\rm H}^{\rm D}$ only qualitatively and that the experimental and theoretical dependences of $\delta\rho_{xy}/\rho_{\rm H}^{\rm D}$ on temperature disagree considerably. Still, the transition from the ballistic to diffusion regime in the behavior of the Hall effect is also clearly seen in the curves in Fig. 3, the lack of perfect agreement being most likely due to the neglect of the weak scattering anisotropy.

3. Metal–insulator transition and quantum corrections to the 2D EG conductivity in the Si/SiGe heterostructure [14]

It has been about ten years since the silicon structure metal–insulator–semiconductor (MIS) with a 2D EG was first found [4] to undergo the metal–insulator transition (MIT) forbidden in the one-parameter scaling model [15]. However, it is still unclear whether this is a phase transition. Although publications abound on the metal–insulator transition in various types of 2D ESs, there has not yet been any report of such a transition in a Si/SiGe heterojunction with a 2D EG, which is all the more unfortunate because this would allow a comparison with what has been seen on silicon MIS structures. These two systems, while totally alike in their electronic spectra, differ in the structure of the scattering potential (which is primarily short-range in silicon MISs and has a long-range component in Si/SiGe heterostructures), and hence the difference in the behavior of these systems can provide information on the role played by the dominant scattering mechanism in the electron–electron interaction.

Our experiments involved Si/SiGe heterostructures grown by molecular beam epitaxy [12], with the electron density $N_{\rm s} = (3.5-6.23) \times 10^{11}$ cm^{-2} and the maximum electron mobility $\mu = 6 \times 10^5$ cm^2 V^{-1} s^{-1}. The transport measurement employed a standard four-probe technique using a low-frequency (10 Hz) small-amplitude (0. 1 μA) ac to avoid heating effects.

The metal–insulator transition is usually observed by measuring the temperature dependence of conductivity at various concentrations of 2D electrons. The concentration in this case was varied by varying the shutter voltage. In our experiments, samples based on a 2D EG containing Si/SiGe heterojunctions were brought from their initial insulating state (which was achieved by cryostatically cooling them to the base temperature) to the metallic state (which proved to be very stable) by applying a succession of specially dosed short-duration LED pulses.

Figure 4 shows the temperature dependence of the resistance for various values of the electron concentration. The transition between the insulating, $d\rho_{xx}/dT < 0$, and metallic, $d\rho_{xx}/dT > 0$, behavior shown in this figure is the first observation of this kind in a Si/SiGe heterostructure with a 2D electron gas. At the electron concentration about 4.05×10^{11} cm^{-2}, there is a sort of boundary between these states, corresponding to the sample resistance $\approx 0.3h/e^2$. The temperature dependence of resistance corresponding to this boundary state is not monotonic (Fig. 4c). As its counterparts in other 2D systems, the observed metal–insulator transition has so far defied explanation. A theoretical analysis is possible only for states with small $r_{\rm s}$ and $\rho_{xx} \ll h/e^2$, and this is precisely where considerable progress has been made in understanding the nature of corrections to the Drude conductivity due to the electron–electron interaction. We now turn to a detailed discussion of this class of phenomena found in samples based on the Si/SiGe heterostructure with a 2D EG.

As noted above, there are two major types of corrections to the conductivity of a 2D electron system: weak localization corrections and those due to the electron–electron interaction. The weak localization correction can be written as [1]

$$\Delta\sigma_{xx}^{\rm wl} = \alpha p \, \frac{e^2}{h} \ln\left(\frac{k_{\rm B}T\tau}{\hbar}\right),$$

where the phase coherence time is assumed to vary with temperature as T^{-p}, and the amplitude α is taken to be unity for ordinary scattering.

Further, according to Ref. [5], the interaction-induced correction at arbitrary $k_{\rm B}T\tau/\hbar$ is given by

$$\Delta\sigma_{xx}^{\rm ee} = \delta\sigma_{\rm C} + 15\delta\sigma_{\rm T},$$

where

$$\delta\sigma_{\rm C} = \frac{e^2}{\pi\hbar} \, \frac{k_{\rm B}T\tau}{\hbar}\left(1 - \frac{3}{8} \, f(T\tau)\right) - \frac{e^2}{2\pi^2\hbar} \ln\left(\frac{1}{T\tau}\right)$$

and

$$\delta\sigma_{\rm T} = \frac{F_0^\sigma}{(1+F_0^\sigma)} \, \frac{e^2}{\pi\hbar} \, \frac{T\tau}{\hbar}\left(1 - \frac{3}{8} \, t\left(T\tau; F_0^\sigma\right)\right) - \left(1 - \frac{1}{F_0^\sigma}\ln\left(1+F_0^\sigma\right)\right) \frac{e^2}{2\pi^2\hbar} \ln\left(\frac{1}{T\tau}\right)$$

are the respective corrections for the interactions in the charge and triplet channels [see Ref. [5] for the exact expressions for the functions $f(T\tau)$ and $t(T\tau; F_0^\sigma)$].

We note that the expression above accounts for the fact that the electronic spectrum of Si is doubly valley-degenerate

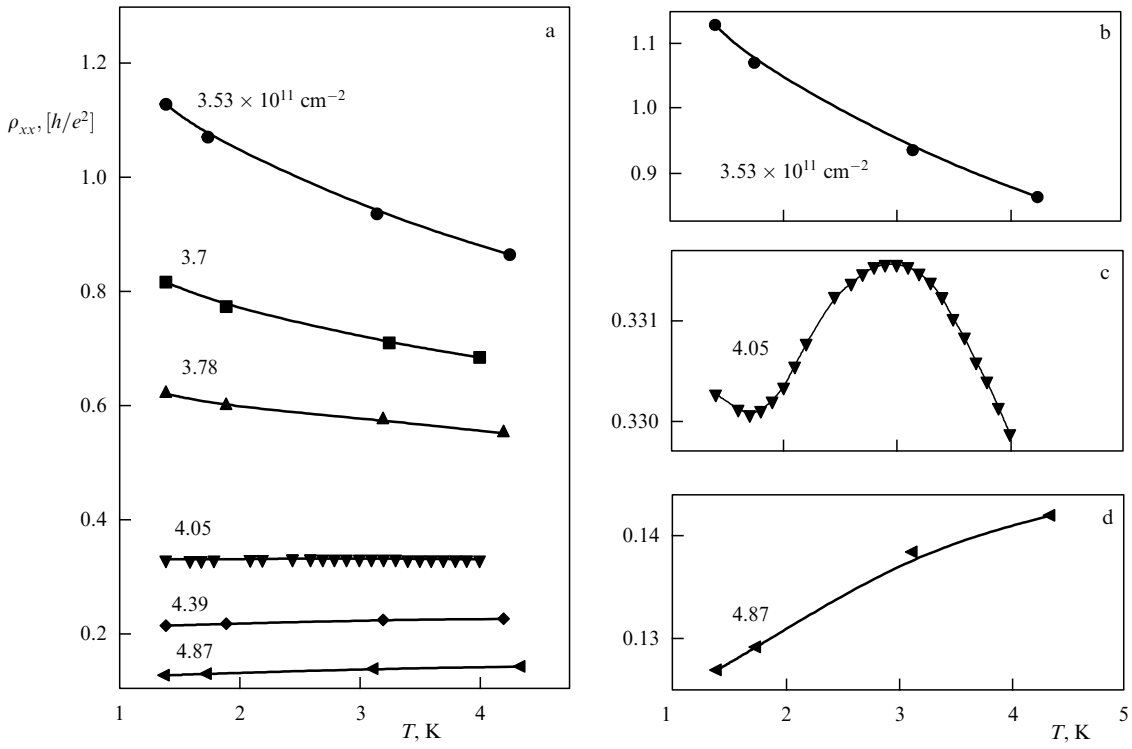

Figure 4. (a) Resistance as a function of temperature for various values of concentration. (b – d) Some of the curves of (a) shown magnified.

near the (100) surface, increasing the numerical factor in front of the triplet term from 3 to 15. In the diffusion limit, the correction due to the interaction reduces to the familiar logarithmic correction [2], whereas in the ballistic and intermediate regime, it is linear in temperature, with the sign and slope dependent on the coupling constant.

Figure 5a shows typical magnetoresistance (MR) curves measured at different temperatures after the electron concentration has been saturated to its maximum by LED radiation. In this state, the electron mobility is $\mu = 61800\ \mathrm{cm^2\,V^{-1}\,s^{-1}}$ and the electron concentration is $N_s = 6.23 \times 10^{11}\ \mathrm{cm^{-2}}$ (corresponding to $r_s \approx 6.7$). We note that for $r_s > 1$, the functional relation between the parameter r_s and the constant F_0^σ is unknown. In Fig. 5b, we show the temperature dependence of conductivity in a zero magnetic field. It is seen that the dependence is linear for $T \geqslant 1.25$ K and saturates at lower temperatures. The Drude conductivity is determined by extrapolating the linear part of the dependence to $T = 0$, and its corresponding momentum relaxation time is $\tau = 6.8 \times 10^{-12}$ s. This means that $T\tau = 0.89T$ and hence the sample under study is either in the intermediate or in the ballistic regime in the temperature range 0.4 – 2.7 K.

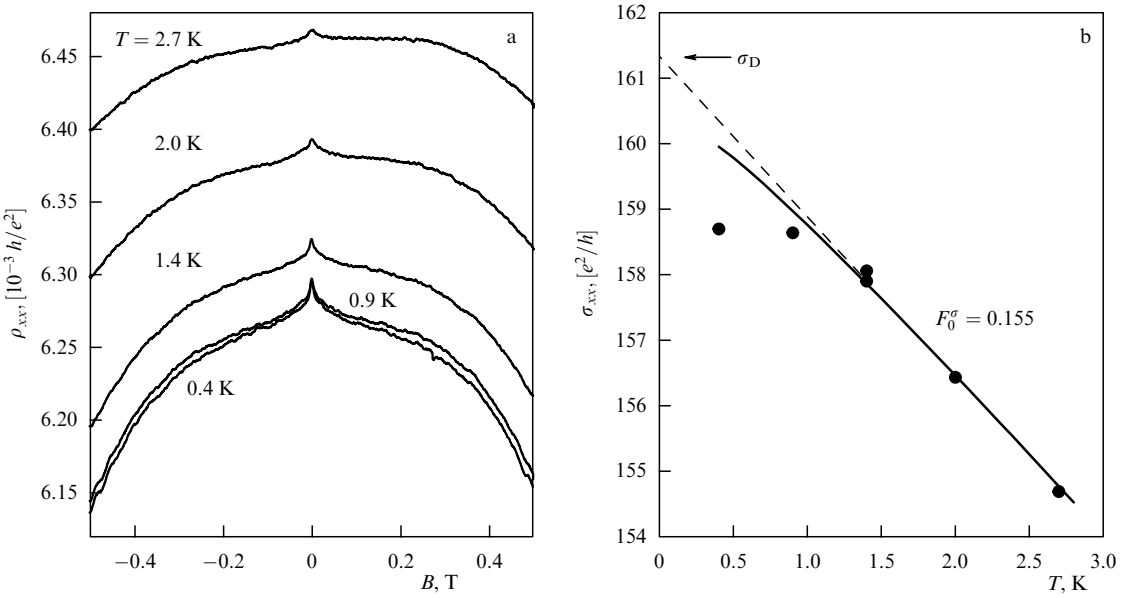

Figure 5. (a) Magnetoresistance at different temperatures. (b) Conductivity as a function of temperature for $B = 0$. Solid curve is the theoretical behavior.

The solid curve in Fig. 5b is the theoretical dependence obtained by adding the weak localization correction and that due to the interaction. It took only one fitting parameter, $F_0^\sigma = -0.155$, to fit the curve to experiment. The weak localization factor $\alpha p = 1.5$ was derived from the sample's weak-magnetic-field behavior. The value $F_0^\sigma = -0.155$ obtained by fitting turns out to be smaller than the corresponding quantities in silicon MIS structures with similar values of r_s by a surprisingly large factor of about two [10]. In our view, this results from the range difference mentioned above between the scattering potentials in these two silicon systems. According to Ref. [5], the temperature-linear interaction-induced correction to the conductivity results from the electron scattering by Friedel density oscillations due to a short-range scattering potential. This type of scattering occurs, for example, in silicon MIS structures. In our samples, the one-particle scattering time τ_q determined from the Shubnikov–de Haas amplitude turns out to be six times smaller than the momentum relaxation time, implying that both types of disorder are present in the samples. Although one might expect that the theory in Ref. [5] is inadequate for describing the experiment in this case, good agreement between theory and experiment is found for $T \geqslant 1.25$ K. One explanation may be the predominance of short-range scattering in a zero magnetic field. As regards the saturation effect observed at low temperatures, it has already been reported elsewhere [16], where intervalley scattering and the lifting of the degeneracy of a zero magnetic field were cited as possible reasons for such behavior.

We next turn to our transverse magnetoresistance results (Fig. 5a). In the diffusion regime, it is known that the zero-magnetic-field interaction-induced correction to conductivity, $\Delta\sigma_{xx}^{ee}(T)$, also retains its form in classically strong magnetic fields, leading to a negative parabolic magnetoresistance of the form $\rho_{xx}(B) = \rho_D + \rho_D^2(\mu B)^2\Delta\sigma_{xx}^{ee}(T)$ for $\omega_c\tau > 1$. Unlike the diffusion regime, the situation with the intermediate and ballistic regimes has received little attention until recently. In particular, it remained unclear whether zero-field corrections remain the same in strong magnetic fields. Recently, a new theory was proposed [7], which calculates magnetoresistance in a strong magnetic field for arbitrary values of $k_B T\tau/\hbar$. Analysis is carried out for both mixed scattering and a smoothly varying scattering potential alone, and it is shown that in both cases, the interaction leads to a parabolic MR similar to that given above except that $\Delta\sigma_{xx}^{ee}(T)$ is expressed as

$$\Delta\sigma_{xx}^{ee}(T) = -\frac{2}{\pi}\left[G_F\left(k_B T\tau/\hbar\right) - G_H\left(k_B T\tau/\hbar; F_0^\sigma\right)\right],$$

where $G_F(k_B T\tau/\hbar)$ and $G_H(k_B T\tau/\hbar; F_0^\sigma)$ are respectively the exchange and triplet contributions, whose form is dependent, among other things, on what scattering mechanism is at work in the system. The exact expressions for these functions can be found in Ref. [7].

The general features (in particular, the negative parabolic MR) seen in the experimental dependences confirm the conclusion about the presence of a magnetic-field-independent correction. Indeed, the experimental curves obtained following the suppression of the weak localization correction show a relatively flat region, which, according to Ref. [7], corresponds to the suppression at low magnetic fields of the backscattering due to the presence of a long-period scattering potential. At higher magnetic fields, the increased probability of backscattering restores the interaction, leading to negative parabolic MR.

For our sample, the condition $\omega_c\tau = 1$ is satisfied for $B = 0.16$ T, with a parabolic MR observed in classically strong fields. Moreover, all the dependences, except for the curve for $T = 0.4$ K, were measured in magnetic fields for which the influence of the Zeeman effect is negligible. Under these conditions, the predictions of the theory in Ref. [7] apply to our experiment. The dots in Fig. 6a show the resistance as a function of B^2 and in Fig. 6b show the interaction-induced corrections to conductivity, $\Delta\sigma_{xx}^{ee}(T)$, obtained from the slope of the linear portion of the dependences in Fig. 6a. Also shown in Fig. 6b are two theoretical curves from Ref. [7], one of which (*1*) is obtained on the assumption of a smooth scattering potential alone, and the other (*2*) is drawn for the

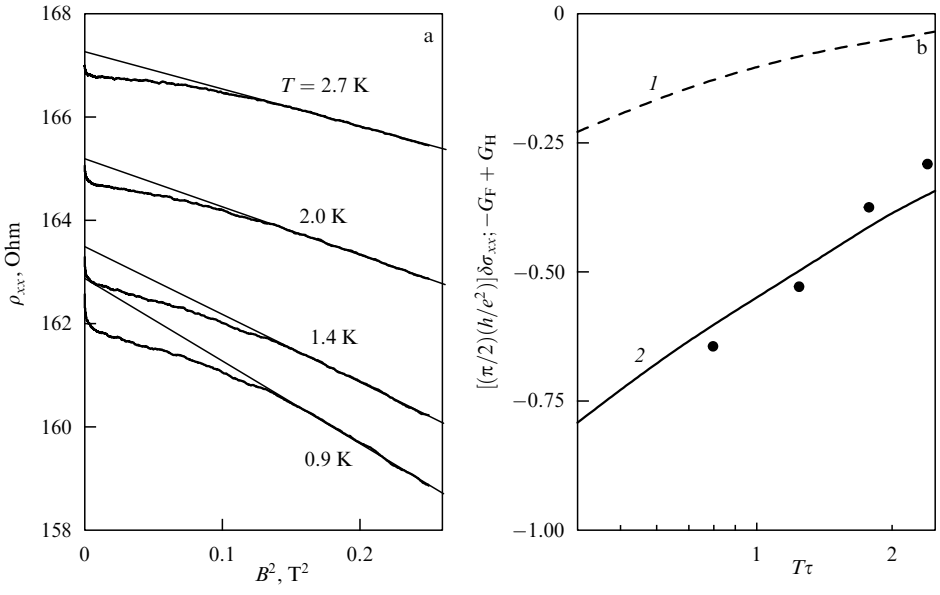

Figure 6. (a) Magnetoresistance as a function of B^2. (b) Experimentally determined correction $\Delta\sigma_{xx}^{ee}(T)$ (dots) and theoretical dependences for it: curve *1* — $F_0^\sigma = -0.15$, smoothly varying scattering potential; curve *2* — $F_0^\sigma = -0.16$, mixed scattering, $\gamma = 5$.

case of mixed scattering. In the latter case, a parameter γ is introduced to describe the relative contribution of each type of scattering [7]. It is seen that whereas assuming scattering by a long-period potential alone leads to disagreement with experiment, good agreement is obtained in the mixed scattering case. Thus, our analysis points to the correct description of scattering as a necessary condition for adequately describing interaction-induced corrections to conductivity — whether in a zero magnetic field or in strong magnetic fields leading to parabiotic magnetoresistance.

References

1. Lee P A, Ramakrishnan T V *Rev. Mod. Phys.* **57** 287 (1985)
2. Altshuler B L, Aronov A G, in *Electron-Electron Interactions in Disordered Systems* (Modern Problems in Condensed Matter Sciences, Vol. 10, Eds A L Efros, M Pollak) (Amsterdam: North-Holland, 1985) p. 1
3. Finkel'shtein A M *Zh. Eksp. Teor. Fiz.* **84** 168 (1983) [*Sov. Phys. JETP* **57** 97 (1983)]; *Pis'ma Zh. Eksp. Teor. Fiz.* **40** 63 (1984) [*JETP Lett.* **40** 796 (1984)]
4. Kravchenko S V et al. *Phys. Rev. B* **50** 8039 (1994)
5. Zala G, Narozhny B N, Aleiner I L *Phys. Rev. B* **64** 214204 (2001)
6. Zala G, Narozhny B N, Aleiner I L *Phys. Rev. B* **64** 201201 (2001)
7. Gornyi I V, Mirlin A D *Phys. Rev. Lett.* **90** 076801 (2003); *Phys. Rev. B* **69** 045313 (2004)
8. Gold A, Dolgopolov V T *Phys. Rev. B* **33** 1076 (1986)
9. Proskuryakov Y Y et al. *Phys. Rev. Lett.* **89** 076406 (2002)
10. Shashkin A A et al. *Phys. Rev. B* **66** 073303 (2002)
11. Kvon Z D et al. *Phys. Rev. B* **65** 161304 (2002)
12. Olshanetsky E B et al. *Phys. Rev. B* **68** 085304 (2003)
13. Renard V T et al. *Phys. Rev. B* **72** 075313 (2005)
14. Olshanetsky E B et al. *Europhys. Lett.* **71** 665 (2005)
15. Abrahams E et al. *Phys. Rev. Lett.* **42** 673 (1979)
16. Brunthaler G et al., cond-mat/0207170